PCCP

ROYAL SOCIETY OF CHEMISTRY

PAPER

View Article Online
View Journal | View Issue

Cite this: *Phys. Chem. Chem. Phys.*, 2024, **26**, 21530

Ab initio study of temperature-dependent piezoelectric and electronic properties of thermally stable $GaPO_4$†

Xiaoqing Yang, [ab] Pan Guo, [b] Shunbo Hu, [b] Zhibin Gao, [c] Wenliang Yao, [b] Jinrong Cheng, [b] Samuel Poncé, [de] Baigeng Wang [a] and Wei Ren *[b]

Received 4th June 2024,
Accepted 23rd July 2024

DOI: 10.1039/d4cp02270j

rsc.li/pccp

Gallium-phosphate ($GaPO_4$) is one of the ultra-high thermally stable piezoelectric materials with a high critical temperature of 1206 K. Here, first principles calculations with quasi-harmonic approximation are performed to study thermal and other physical properties of α-$GaPO_4$. For the electronic structure, we focus on the electron–phonon interaction and lattice expansion effects on the temperature-dependent band gap, which plays a significant role in zero-point renormalization. Significantly, the large piezoelectric constants e_{11} primarily comes from intrinsic sensitivity of Ga and O sites to axial strain, while P atoms contribute little, which remains true in other quartz-like type APO_4 (A = B, Al, In). Our work provides an insight into the temperature-dependent electronic and piezoelectric properties of α-$GaPO_4$ and motivates its applications in a high temperature environment.

1. Introduction

Gallium phosphate ($GaPO_4$) is a multifunctional oxide with a wide bandgap of 7.1 eV.[1] It is attractive for high-temperature semiconductor device of high resistivity, superior piezoelectric, high mechanical quality factor, and physical properties that barely change up to 1206 K. Furthermore, the existence of temperature-compensated orientations for bulk acoustic waves (BAW) and surface acoustic waves (SAW) is a valuable feature of $GaPO_4$ for applications in communications, frequency control, and signal processing.[2–4] Apart from this, it can be applied to make high-temperature ultrasonic positioning detectors used in nuclear reactors, fuel injection piezoelectric valves used in internal combustion engines, as well as play an important role in aerospace, petroleum exploration, and high-temperature piezoelectric acceleration sensors.[4–6]

Previous reports on $GaPO_4$ are mainly experiment-based. Hamidon *et al.*[7] exploited $GaPO_4$ to prepare SAW devices which can be used satisfactorily for high-temperature, wireless sensing, and tested the long-term stability of working at 434 MHz and a maximum of 600 °C. Several experiments measured the elastic and piezoelectric constants around room temperature and other temperatures with samples made by slow cooling, reverse temperature gradient, high-temperature solution growth, hydrothermal reaction under pH-dependent control methods.[3,8–11] However, theoretical studies of $GaPO_4$ are scarce and limited to predicting zero-temperature properties. Liu *et al.*[12] performed a computational investigation on structural, elastic, and optical properties of $GaPO_4$. Hermet *et al.*[13] calculated the piezoelectric coupling of α-quartz-type MXO_4 compounds (M = B, Al, Ga; X = P, As) with different inter-tetrahedral angles and revealed the origin of piezoelectricity is related to such angles. *Ab initio* studies on the temperature-dependent properties of $GaPO_4$ remain absent.

In this work, we explore the intrinsic properties of $GaPO_4$ as function of temperature ranging from 0 to 1000 K by exploiting density functional theory (DFT) and the quasi-harmonic approximation (QHA). The paper is organized as follows: firstly, based on first-principles calculations, we optimize the structure of α-$GaPO_4$ at 0 K using three different functionals. The lattice constants, piezoelectric properties, and elastic properties of these three structures are compared with experiment. It is found that the PBEsol functional yields a more accurate description of crystal information and shows a better agreement with experimental observations. In the second section, we

[a] *School of Physics and National Laboratory of Solid State Microstructures, Nanjing University, Nanjing 210093, China*
[b] *Physics Department, Materials Genome Institute, State Key Laboratory of Advanced Special Steel, Shanghai Key Laboratory of High Temperature Superconductors, International Centre for Quantum and Molecular Structures, Shanghai University, Shanghai 200444, China. E-mail: renwei@shu.edu.cn*
[c] *State Key Laboratory for Mechanical Behavior of Materials, Xi'an Jiaotong University, Xi'an 710049, China*
[d] *European Theoretical Spectroscopy Facility, Institute of Condensed Matter and Nanosciences, Université Catholique de Louvain, Chemin des Étoiles 8, B-1348 Louvain-la-Neuve, Belgium*
[e] *WEL Research Institute, avenue Pasteur, 6, 1300 Wavre, Belgium*

† Electronic supplementary information (ESI) available. See DOI: https://doi.org/10.1039/d4cp02270j

evaluate the volumetric thermal expansion coefficient of α-$GaPO_4$ crystal in the range of 300–1000 K based on the QHA method and the *ab initio* molecular dynamics (AIMD) method (Fig. S1, ESI†). The simulation results obtained using the QHA are closer to the experimental values as compared to that from AIMD. Consequently, we use the α-$GaPO_4$ structure obtained from the QHA method for further temperature-related investigations. Besides, the corresponding AIMD simulations for α-$GaPO_4$ are provided in Fig. S2 (ESI†), which show that the structures at 300 K, 700 K, 1000 K are all stable and similar. The third section investigated renormalization of the electronic structure of α-$GaPO_4$ over a wide temperature range, contributed by lattice expansion and electron–phonon interactions. Some representative one-shot configurations of $GaPO_4$ with temperature are shown in Fig. S3 (ESI†). Moreover, based on QHA calculations, we also display temperature-dependent elastic properties and piezoelectric constants.

2. Computational method

All computations are based on the DFT[14] as implemented in the vienna *ab initio* simulation package (VASP).[15] We employ a plane-wave kinetic energy cutoff of 550 eV, Γ-centered $8 \times 8 \times 4$ k-point mesh, a convergence criterion of 10^{-7} eV for the energy, and 10^{-4} eV $Å^{-1}$ for the Hellmann–Feynman forces on all atoms. For all calculations, the valence state configurations are taken as $3d^{10}4s^24p^1$ for Ga, $3s^23p^3$ for P, $2s^22p^4$ for O, $2s^22p^1$ for B, $3s^23p^1$ for Al, $4d^{10}5s^25p^1$ for In. We use projector-augmented wave (PAW) pseudopotential[16,17] and the generalized gradient approximation (GGA-PBEsol) functional[18,19] for the exchange–correlation potential. The electronic correlation in the d shell of Ga is corrected by the PBEsol+U method[20] (see supplementary figures and tables, ESI†).

Based on the QHA[21,22] and "one-shot" method,[23] we investigate band gaps at finite temperatures that include electron–phonon interaction and volume thermal expansion effects.[24] The procedure can be divided in 5 steps as follows: (1) the structures and volume (V) as a function of temperature are determined using the QHA method. (2) The phonon spectra are calculated using a $3 \times 3 \times 2$ supercell (324 atoms) with the temperature dependent volumes $V(T)$. (3) The band gap at finite temperatures with volumetric effect can be extracted from QHA calculations. (4) One-shot configuration generates a single set of atomic displacements from the equilibrium positions by taking into account the mean absolute phonon displacement influenced by the temperature-dependent phonon occupations. (5) By calculating the band gap of the one-shot configuration, the effect of electron–phonon interactions is revealed. Finally, temperature-dependence of the band gaps including both lattice expansion (LE) and phonon vibration (VIB) effects are predicted. The band gaps at finite temperatures can be extracted from the effective band structure (EBS), which is predicted by unfolding the band energies in the supercell into the primitive cell.

Additionally, piezoelectric constants e_{ij} and elastic constants C_{ij} are derived from density functional perturbation theory[25] at a given temperature. The structures are drawn with the software VESTA.[26] *Ab initio* molecular dynamics (AIMD) simulations were performed in the isothermal–isobaric ensemble (NPT) using a Langevin thermostat for 20 ps with a step of 2 fs, to assess the thermal stability and volume of $GaPO_4$ in the high-temperature range from 300 K to 1100 K, with increments of 200 K.[27,28]

3. Results and discussion

α-$GaPO_4$ is iso-structural with the classical piezoelectric material α-SiO_2. In Fig. 1(a), the crystal structure of SiO_2 transforms

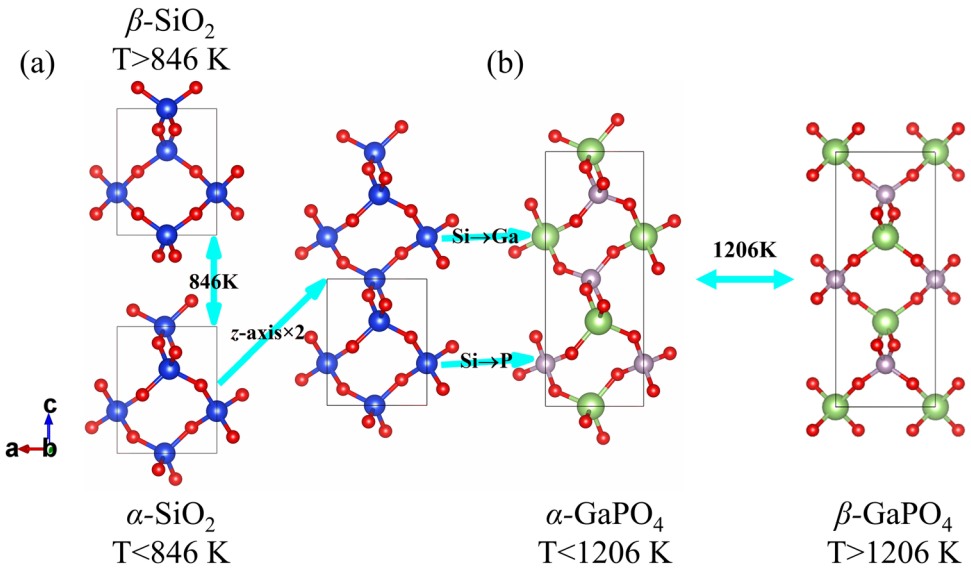

Fig. 1 Crystal structures of the quartz SiO_2 and quartz type $GaPO_4$. (a) The classic phases of α-SiO_2 (at room temperature) and β-SiO_2 (at temperature higher than 846 K). (b) The crystal structures of α-$GaPO_4$ at temperature below and β-$GaPO_4$ higher than 1206 K. The blue, red, green, and gray spheres are Si, O, Ga and P atoms, respectively.

from α-phase (stable at low temperature) to β-phase (stable at high temperature) as the temperature rises over 846 K with the disappearance of piezoelectricity. The α-$GaPO_4$ crystal in Fig. 1(b) can be derived from the 1 × 1 × 2 supercell of α-SiO_2, by replacing Si with Ga and P atoms alternately along the *c* direction. Similar to α-SiO_2, the α-$GaPO_4$ crystal (trigonal symmetry with $P3_121$ space group) remains the stable phase at low temperature. When the temperature is above 1206 K,[29,30] $GaPO_4$ undergoes a structural phase transition to the centrosymmetric β-$GaPO_4$ phase, accompanied by the loss of its piezoelectricity. The exceptionally high piezoelectric critical phase transition temperature renders $GaPO_4$ a promising material for high temperature applications.

Based on DFT, we employ three different functionals to calculate the lattice constants, piezoelectric constants, and elastic constants of α-$GaPO_4$ crystal, as shown in Table 1. The local-density approximation (LDA) and Perdew–Burke–Ernzerhof (PBE) are the standard choice for calculations of periodic crystals.[18,31] PBEsol is designed to yield accurate lattice constants and bulk moduli and may be a better choice for calculating lattice constants of solids.[32] Compared with experimental values, we find that the PBEsol functional describes α-$GaPO_4$ crystal more accurately than other functionals. Concerning the lattice constants *a* and *b*, the errors of PBE and LDA functionals are nearly 2% with respect to experimental values, while using PBEsol functional we obtain the most accurate results with an error within 0.2%. The volume calculated by PBEsol functional is only 0.6% smaller than the experiment. Therefore, we adopt the PBEsol functional to investigate physical properties of $GaPO_4$, with the optimized lattice constants $a = b = 4.91$ Å, $c = 11.10$ Å, $\alpha = \beta = 90^\circ$ and $\gamma = 120^\circ$.

The QHA method deals with the thermal properties of solid materials, which is based on the dependency of the harmonic-approximation level non-interacting phonon frequencies over lattice volume or other thermodynamic constraints.[36,37] The Helmholtz free energy $F(V, T)$ at the QHA level is expressed as

$$F(V, T) = E_0(V) + F_{vib}(V, T) + F_{el}(V, T) \quad (1)$$

where $E_0(V)$ is the energy of the ground state at zero temperature, $F_{vib}(V, T)$ is the vibrational free energy from phonons, $F_{el}(V, T)$ is the contribution of electronic thermal excitations to free energy. According to the free energy of the lattice, the equation of states and all thermodynamic functions of the system can be obtained.

Lattice vibrational free energy $F_{vib}(V, T)$ can be obtained from eqn (2), where $\omega_{q\lambda}$ represents the frequency of the λ-th phonon mode at wave vector q in the first Brillouin zone and k_B is the Boltzmann constant,

$$F_{vib}(V, T) = \sum_{q\lambda}\left[\frac{1}{2}\hbar\omega_{q\lambda} + k_B T \ln\left(1 - e^{-\hbar\omega_{q\lambda}/k_B T}\right)\right] \quad (2)$$

The electronic free energy $F_{el}(V, T)$ is obtained from the electronic entropy S_{el} and energy E_{el} contributions as

$$F_{el} = E_{el} - TS_{el} \quad (3)$$

For the wide-bandgap semiconductor, the electron contribution to the free energy is negligible, hence we ignore the electronic contribution $F_{el}(V, T)$ of eqn (1) in this paper. We calculate the Helmholtz free energy $F(V, T)$ as a function of volume with a temperature step of 100 K, and get the minima of $F(V, T)$, as shown in Fig. 2(a). The Helmholtz free energy is fitted using the Vinet equation:[38]

$$\begin{aligned} P(X, T) &= 3K_0^T\frac{(1 - X)}{X^2}e^{[\eta(1-X)]} \\ \eta &= \frac{3(K_0^{T'} - 1)}{2} \\ X &= (V/V_0)^{1/3}. \end{aligned} \quad (4)$$

As a consequence of lattice thermal expansion (isotropic stretching), the volume of the $F(V, T)$ minimum increases as the temperature is going up. The thermal effects on the equilibrium lattice volume is determined from the equation

$$\Delta V/V_0 = \alpha_V \Delta T \quad (5)$$

Interestingly, $GaPO_4$ displays a negative volume thermal expansion coefficient α_V at low temperatures and a positive volume thermal expansion at higher temperature. The negative thermal expansion at low temperature is a common feature of tetrahedrally coordinated elements such as Si.[39–41] As explaned using a microscopic Gibbs free energy by Biernacki,[41] such negative thermal expansion originates from decreased entropy upon volumetric expansion at low temperature due to the increased low-lying phonon frequencies. Therefore, the lattice

Table 1 Calculated results with different functionals (at 0 K) and experimental values: unit-cell lattice parameters *a*, *b* and *c* (Å), volume (Å^3), piezoelectric constants e_{ij} (C/m^2) and elastic constants C_{ij} (GPa)

Functional	PBE	LDA	PBEsol	Experiment[33–35]
$a = b$	5.01 (1.8%)	4.82 (−2.0%)	4.91 (−0.2%)	4.92
c	11.26 (2.4%)	10.95 (−0.5%)	11.10 (0.9%)	11.00
Volume	244.66 (6.1%)	220.47 (−4.4%)	232.09 (0.6%)	230.60
e_{11}	0.17	0.20	0.18	0.21
e_{14}	0.11	0.11	0.13	0.10
C_{14}	4.90	3.23	4.27	3.91
C_{33}	89.35	111.17	97.73	102.13
C_{44}	36.66	32.84	35.25	37.66
C_{66}	23.15	17.87	21.33	22.38

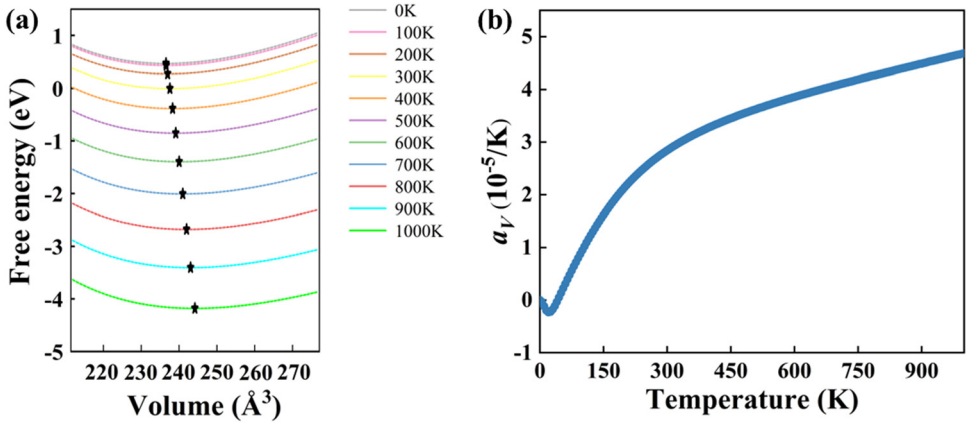

Fig. 2 (a) Helmholtz free energy (minima indicated by star symbols) fitted by Vinet equation. (b) Volumetric thermal expansion coefficient of α-$GaPO_4$.

contracts compared to that at 0 K. The low expansion coefficient of $GaPO_4$ is at the same order of magnitude as that of SiO_2, which makes it suitable and stable for high-temperature applications.

The electronic structures at high temperatures are critical properties to the development of new technologies, but difficult to characterize and measure experimentally. The first principle one-shot method is a recently-developed method to study the temperature-dependent band structures in semiconductors and insulators.[42–45] Temperature dependence of the band structure can be attributed to two main factors, *i.e.* lattice thermal expansion and electron–phonon interaction. The effect of lattice thermal expansion on electronic structures can be predicted through QHA. The electron–phonon interaction, also known as the electron–phonon renormalization (EPR) of the electronic structure, has been explored for various materials, which are typically divided into two categories, namely, the band gap either decreases with increasing temperature due to Varshni effect[46] or the opposite trend due to inverse Varshni effect.[47] Even at absolute zero temperature, electron–phonon interactions may also modify the band gap, which is commonly referred to as the zero-point renormalization (ZPR). Considering EPR effect, the change of electronic energy at finite temperatures consists of three parts:[48]

$$\Delta E_{nk}(T) = \Delta E_{nk}^{VIB}(0) + \Delta E_{nk}^{VIB}(T) + \Delta E_{nk}^{LE}(T) \quad (6)$$

The three terms on the right of eqn (6) relates to ZPR at 0 K, EPR from lattice vibration at finite temperature T and contribution from lattice thermal expansion at T.

Based on the simulated lattice thermal expansion of α-$GaPO_4$ at the QHA level, we further evaluate the temperature-dependent renormalization of the band gap due to electron–phonon interactions and lattice thermal expansion in a range from 0 K to 1000 K, which remain unknown to experimentalists. At the GGA-PBEsol level, the equilibrium lattice of α-$GaPO_4$ possesses a wide band gap of 4.60 eV at 0 K, which is underestimated with respect to the experimental value. As compared to the band structure without EPR effect, the ZPR in $GaPO_4$ corrects the band gap by −0.87 eV. The strength of ZPR varies among materials in Table 2. Nery *et al.*[49] proved that for the strongly polarized materials, long-range Fröhlich-like interactions contribute majorly to the total ZPR. We note that the adiabatic one-shot method used here with a small supercell provide sound results by including some anharmonic effect,[50,51] but non-adiabatic theories are expected to yield more accurate results.

In the case of polarized $GaPO_4$, we individually calculate the temperature-dependent energy gap including only LE effect and only phonon VIB effect, as well as including both LE and VIB effects in Fig. 3(a). With only LE, the energy gap is almost unchanged (only by −0.03 eV from 0 K to 1000 K) when the temperature increases. However, the band gap shows a significant decreasing trend by only VIB effect (reduced by 1.27 eV from 0 K to 1000 K). When considering both LE and VIB effects, the energy gap lowers by about 1.34 eV due to the temperature increase. This behavior is consistent with previous studies on the temperature dependence of the electronic structure of diamond and AlN.[51] Table S1 (ESI†) shows the electronic gap values that include VIB or LE effect of α-$GaPO_4$.

We fit the simulated decline of band gap over increasing temperature relation against Varshni formula.

$$E_g(T) = E_g(0) - \frac{\alpha T^2}{T + \beta}, \quad (7)$$

where $E_g(0)$ is the band gap at 0 K that includes EPR effect, and α and β are fitting parameters of a given material. As shown in the inset of Fig. 3(a), fitting parameters α (1.6×10^{-3} eV/K) and β (149.4 K) are both positive, similar to common semiconductors such as Si, Ge, and GaAs.[53] There are two main reasons leading to such phenomenon, namely, the higher temperature increases both atomic vibrations and interatomic distances,

Table 2 Band-gap ZPR for $GaPO_4$ and other materials with high/low ZPR corrections

High ZPR	Value (eV)	Low ZPR	Value (eV)
$GaPO_4$	−0.87	AlAs[52]	−0.074
SiO_2[50,52]	−0.58	ZnO[52]	−0.18
Diamond[24]	−0.61	AlP[52]	−0.096
BeO[52]	−0.73	CdS[52]	−0.067

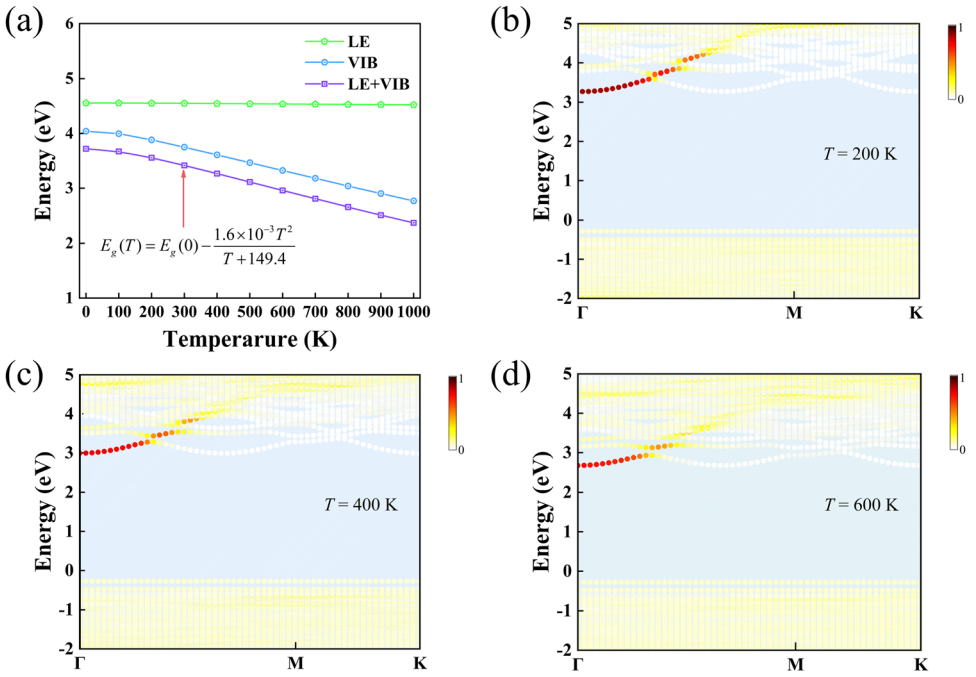

Fig. 3 (a) Temperature-dependence of the direct band gaps including only lattice expansion (LE) effect (green line), only phonon vibration (VIB) effect (blue line), and both LE and VIB effects (purple line). Effective band structures with LE and VIB effects *versus* temperature at (b) 200 K, (c) 400 K and (d) 600 K, with the fermi energy set to zero.

profoundly altering the electron–phonon interaction and its impact on band gap.

We then calculate the temperature-dependent EBS by unfolding the band energies of the supercell into the primitive cell. The EBS that takes EPR effect into account exhibits band gap values of 3.56 eV, 3.27 eV and 2.96 eV, respectively, as shown in Fig. 3(b)–(d). The shift of CBM makes a major contribution to the decrease in energy gap with temperature. Overall, the contribution from electron–phonon interaction at finite temperatures dominates in the non-negligible electronic renormalization. In addition, DFT+U is a method that was proposed to improve the description of systems with strongly correlated d or f electrons.[54] We test the effect of Hubbard U values on lattice parameters and band gap in Fig. S4 (ESI†).

As an excellent and ultra-high thermally stable piezoelectric, there are already plenty reports about piezoelectric response for $GaPO_4$.[55,56] To analyze the origin of its promising piezoelectricity, we calculate the piezoelectric constants on APO_4 (A = B, Al, Ga, In) using the formulae:

$$e_{11} = e_{11,i} + e_{11,c} \quad (8)$$

$$e_{11,i} = \sum_s \frac{ea}{V} Z_{11} \frac{\partial u_1(s)}{\partial \eta_1}. \quad (9)$$

here, s runs over the atoms in the unit cell, e is the electronic charge, a is lattice parameter in x direction, V represents unit cell volume, Z_{11} is Born effective charge, u_1 is atomic internal coordinates and η_1 is uniaxial strain in x direction. The first term $e_{11,i}$ evaluates the piezoelectric response from ion relaxation due to macroscopic strain. The second term $e_{11,c}$ is the clamped-ion contribution from the electronic response to strain. As shown in Table S4 (ESI†), the clamped-ion term $e_{11,c}$ of APO_4 is rather similar, contributing little to the difference of total e_{11}. Clamped-ion part quantifies the degree to which the Wannier centers deviate from following the homogeneous strain. This negative behavior can be attributed to the phenomenon known as the "lag of Wannier center" effect.[57] By decomposing the relaxed-ion term of three kinds of atoms, Fig. 4 display the internal parameter response to strain. The internal coordinate u of P atom is almost unchanged with strain in all APO_4, while the gradients of A element and O element become larger (from B to In). We find that this strong internal coordinate change mainly comes from A1–O and A3–O tetrahedron in Fig. 4, while A2–O tetrahedron is symmetric in the x direction. In the huge piezoelectric response $GaPO_4$, the $\partial u_1/\partial \eta_1$ of Ga atoms have 43.5% contribution, P atoms have 6.5% contribution and O atoms have 50.0% contribution. For the highest e_{11} of $InPO_4$, the internal coordinate change of In atoms contribute 52.9%, while that of P atoms contribute −2.9% and O atoms contribute 50.0%. Our calculations confirm that significant e_{11} in quartz-like APO_4 system primarily arises from sensitive response of A sites and O sites coordinates to axial strain. We also examine the temperature-dependent variations of the piezoelectric modulus d_{ij} and electromechanical coupling e_{ij} of $GaPO_4$, ranging from 300 K to 900 K, as shown in Fig. S8 (ESI†).

4. Conclusions

In our study, we employ density functional theory calculations together with quasi-harmonic approximation to investigate the

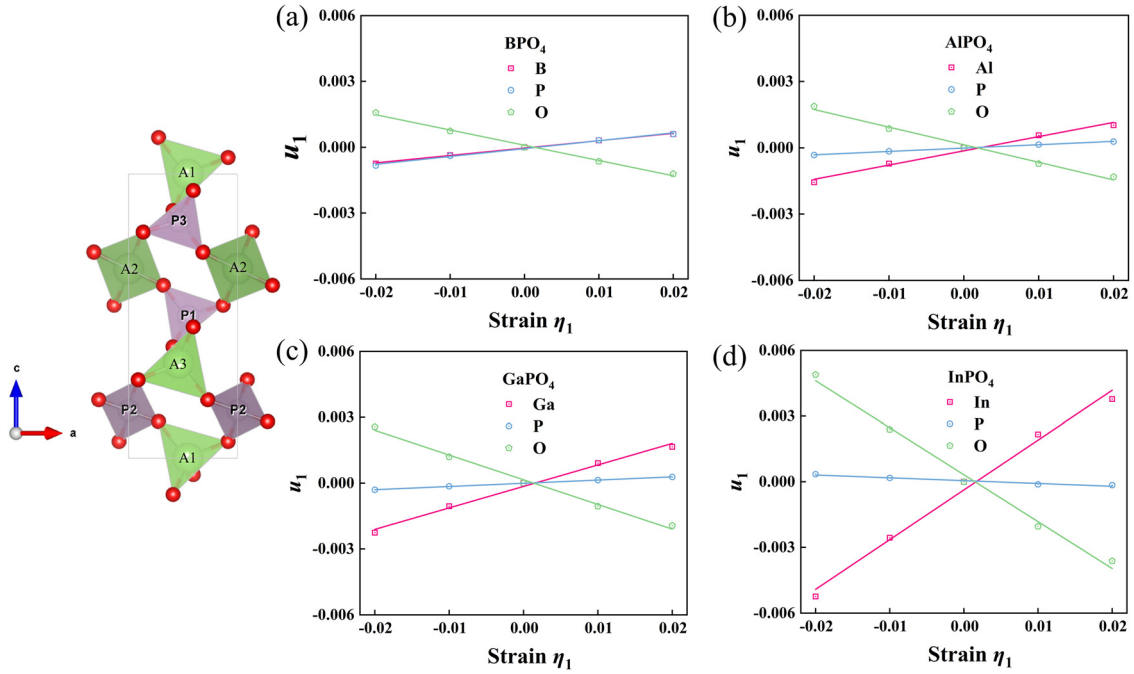

Fig. 4 Internal coordinates u_1 of atoms change as a function of strain in the x direction of (a) BPO_4, (b) $AlPO_4$, (c) $GaPO_4$ and (d) $InPO_4$. Red line is internal coordinate changes of the sum of A (A = B, Al, Ga, In) element (3 atoms in a unit cell). Blue line is internal coordinate changes of the sum of P element (3 atoms in a unit cell). Green line is internal coordinate changes of the sum of O element (12 atoms in a unit cell).

temperature-dependent physical properties of quartz-like $GaPO_4$. Specifically, we focus on the effects of electron–phonon interaction and lattice expansion on the temperature-dependent electronic energy gap. Our findings reveal that the energy gap of $GaPO_4$ decreases with increasing temperature. By including both the electron–phonon interaction and lattice expansion, we observe that the band gap reduces significantly by 1.34 eV as the temperature rises from 0 to 1000 K, considering the zero-point renormalization of 0.87 eV. Furthermore, our study reveals that the large piezoelectric e_{11} is governed by intrinsic sensitivity of Ga and O atoms to axial strain, while P atoms contribute little. Overall, our work provides a comprehensive understanding to the fundamental properties of $GaPO_4$ across a wide temperature range. These insights offer valuable guidance for ongoing experimental efforts in the field of ultra-high temperature applications.

Data availability

The data underlying this article are available in the article and in its online ESI.†

Conflicts of interest

The authors declare that they have no conflict of interest.

Acknowledgements

This work was supported by the National Natural Science Foundation of China (12074241, 12311530675, 52120204), Key Research Project of Zhejiang Laboratory (No. 2021PE0AC02), the Science and Technology Commission of Shanghai Municipality (22XD1400900, 20501130600, 21JC1402600, 21JC1402700), Shanghai Technical Service Center of Science and Engineering Computing, and High Performance Computing Center, Shanghai University. Z. G. acknowledges the support of the National Natural Science Foundation of China (12104356), China Postdoctoral Science Foundation (No. 2022M712552), the Fundamental Research Funds for the Central Universities, and HPC Platform of Xi'an Jiaotong University. S. P. acknowledges support from the Fonds de la Recherche Scientifique de Belgique (FRS-FNRS) and the Walloon Region in the strategic axe FRFS-WEL-T.

References

1 J. D. Pedarnig, M. Peruzzi, H. Salhofer, R. Schwodiauer, W. Reichl and J. Runck, F_2-laser patterning of $GaPO_4$ resonators for humidity sensing, *Appl. Phys. A*, 2005, **80**(7), 1401–1404.
2 P. W. Krempl, Quartz homeotypic gallium-orthophosphate-a new high tech piezoelectric material, *IEEE Int. Ultrason. Symp.*, 1994, **2**, 949–954.
3 P. Davulis, J. A. Kosinski and M. P. D. Cunha, $GaPO_4$ stiffness and piezoelectric constants measurements using the combined thickness excitation and lateral field technique, *IEEE Int. Freq. Control Symp. Expo.*, 2006, 664–669.
4 C. Reiter, P. W. Krempl, H. Thanner, W. Wallnöfer and P. M. Worsch, Material properties of $GaPO_4$ and their relevance for applications, *Ann. Chim. Sci. Mat.*, 2001, **26**(1), 91–94.

5 R. E. Eitel, C. A. Randall, T. R. Shrout and S.-E. Park, Preparation and characterization of high temperature perovskite ferroelectrics in the solid-solution $(1-x)BiScO_3$–$xPbTiO_3$, *Jpn. J. Appl. Phys.*, 2002, **41**, 2099–2104.
6 J.-R. Cheng, W. Zhu, N. Li and L. E. Cross, Fabrication and characterization of $xBiGaO_{3-(1-x)}PbTiO_3$: a high temperature reduced Pb-content piezoelectric ceramic, *Mater. Lett.*, 2003, **57**(13–14), 2090–2094.
7 M. N. Hamidon, V. Skarda, N. White, F. Krispel, P. Krempl, M. Binhack and W. Buff, High-temperature 434 MHz surface acoustic wave devices based on $GaPO_4$, *IEEE Trans. Ultrason. FERR*, 2007, **53**, 2465–2470.
8 P. Armand, M. Beaurain, B. Ruffle, B. Menaert, D. Balitsky, S. Clement and P. Papet, Characterizations of piezoelectric $GaPO_4$ single crystals grown by the flux method, *J. Cryst. Grow.*, 2008, **310**(7–9), 1455–1459.
9 F. Krispel, G. Schleinzer, P. W. Krempl and W. Wallnöfer, Measurement of the piezoelectric and electrooptic constants of $GaPO_4$ with a michelson interferometer, *Ferroelectrics*, 1997, **202**(1), 307–311.
10 M. Beaurain, P. Armand, J. Detaint, B. Menaert, D. Balitsky and P. Papet, Elastic characterizations of α-$GaPO_4$ single crystals grown by the flux method, *J. Phys.: Condens. Matter*, 2008, **20**(2), 025226.
11 C.-S. Yang, C.-J. Chen and X.-H. Lin, Morphology evolution of $GaPO_4$ mesocrystals in a nonionic triblock copolymer system by pH-dependent control, *New J. Chem.*, 2007, **31**(3), 363–369.
12 Q. Liu, Z. Liu, L. Feng and H. Tian, First-principles study of structural, elastic, electronic and optical properties of orthorhombic $GaPO_4$, *Solid State Sci.*, 2011, **13**(5), 1076–1082.
13 P. Hermet, J. Haines, J. P. Aubry and O. Cambon, Origin and mechanism of piezoelectricity in α-Quartz-type $M^{III}X^{V}O_4$ Compounds (M = B, Al, or Ga; X = P or As), *J. Phys. Chem. C*, 2016, **120**(47), 26645–26651.
14 B. Y. Tong and L. J. Sham, Application of a self-consistent scheme including exchange and correlation effects to atoms, *Phys. Rev.*, 1966, **144**(1), 1–4.
15 G. Kresse and J. Hafner, Ab initio molecular dynamics for liquid metals, *Phys. Rev. B*, 1993, **47**(1), 558–561.
16 P. E. Blöchl, Projector augmented-wave method, *Phys. Rev. B*, 1994, **50**(24), 17953–17979.
17 G. Kresse and D. Joubert, From ultrasoft pseudopotentials to the projector augmented-wave method, *Phys. Rev. B*, 1999, **59**(3), 1758–1775.
18 P. Haas, F. Tran and P. Blaha, Calculation of the lattice constant of solids with semilocal functionals, *Phys. Rev. B*, 2009, **79**, 8.
19 K. Burke, J. P. Perdew and M. Ernzerhof, Why the generalized gradient approximation works and how to go beyond it, *Int. J. Quantum Chem.*, 1997, **61**(2), 287–293.
20 A. Jain, G. Hautier, S. P. Ong, C. J. Moore, C. C. Fischer, K. A. Persson and G. Ceder, Formation enthalpies by mixing GGA and GGA + U calculations, *Phys. Rev. B*, 2011, **84**(4), 045115.
21 J. D. Althoff, P. B. Allen, R. M. Wentzcovitch and J. A. Moriarty, Phase diagram and thermodynamic properties of solid magnesium in the quasiharmonic approximation, *Phys. Rev. B*, 1993, **48**(18), 13253–13260.
22 A. N. Al-Rawi, A. Kara, P. Staikov, C. Ghosh and T. S. Rahman, Validity of the quasiharmonic analysis for surface thermal expansion of Ag(111), *Phys. Rev. Lett.*, 2001, **86**(10), 2074–2077.
23 M. Zacharias and F. Giustino, One-shot calculation of temperature-dependent optical spectra and phonon-induced band-gap renormalization, *Phys. Rev. B*, 2016, **94**(7), 075125.
24 F. Giustino, S. G. Louie and M. L. Cohen, Electron-phonon renormalization of the direct band gap of diamond, *Phys. Rev. Lett.*, 2010, **105**(26), 265501.
25 S. Baroni and R. Resta, Ab initio calculation of the macroscopic dielectric constant in silicon, *Phys. Rev. B*, 1986, **33**(10), 7017–7021.
26 K. Momma and F. Izumi, VESTA: a three-dimensional visualization system for electronic and structural analysis, *J. Appl. Crystallogr.*, 2008, **41**(3), 653–658.
27 M. Parrinello and A. Rahman, Crystal structure and pair potentials: A molecular-dynamics study, *Phys. Rev. Lett.*, 1980, **45**(14), 1196–1199.
28 M. Parrinello and A. Rahman, Polymorphic transitions in single crystals: A new molecular dynamics method, *J. Appl. Phys.*, 1981, **52**(12), 7182–7190.
29 O. Cambon and J. Haines, Hydrothermal crystal growth of piezoelectric α-quartz phase of AO_2 (A = Ge, Si) and MXO_4 (M = Al, Ga, Fe and X = P, As): A historical overview, *Crystals*, 2017, **7**, 2.
30 P. Krempl, G. Schleinzer and W. Wallnöfer, Gallium phosphate, $GaPO_4$: a new piezoelectric crystal material for high-temperature sensorics, *Sens. Actuators, A*, 1997, **61**(1), 361–363.
31 B. Hammer, L. B. Hansen and J. K. Nørskov, Improved adsorption energetics within density-functional theory using revised Perdew-Burke-Ernzerhof functionals, *Phys. Rev. B*, 1999, **59**(11), 7413–7421.
32 J. P. Perdew, A. Ruzsinszky, G. I. Csonka, O. A. Vydrov, G. E. Scuseria, L. A. Constantin, X. Zhou and K. Burke, Restoring the density-gradient expansion for exchange in solids and surfaces, *Phys. Rev. Lett.*, 2008, **100**(13), 136406.
33 P. Worsch, P. Krempl, F. Krispel, C. Reiter, H. Thanner and W. Wallnoefer, The temperature-stable piezoelectric material $GaPO_4$ and its sensor applications, *Transducers 01 Eurosensors XV*, 2001, 978–981.
34 J. Haines, O. Cambon, N. Prudhomme, G. Fraysse, D. A. Keen, L. C. Chapon and M. G. Tucker, High-temperature, structural disorder, phase transitions, and piezoelectric properties of $GaPO_4$, *Phys. Rev. B*, 2006, **73**(1), 014103.
35 E. C. Shafer and R. Roy, Studies of silica-structure phases: I, $GaPO_4$, $GaAsO_4$, and $GaSbO_4$, *J. Am. Ceram. Soc.*, 1956, **39**(10), 330–336.

36 B. B. Karki and R. M. Wentzcovitch, Vibrational and quasi-harmonic thermal properties of CaO under pressure, *Phys. Rev. B*, 2003, **68**(22), 224304.
37 C. H. Hu, Y. M. Wang, D. M. Chen, D. S. Xu and K. Yang, First-principles calculations of structural, electronic, and thermodynamic properties of Na_2BeH_4, *Phys. Rev. B*, 2007, **76**(14), 144104.
38 P. Vinet, J. Ferrante, J. H. Rose and J. R. Smith, Compressibility of solids, *J. Geophys. Res.: Solid Earth*, 1987, **92**(B9), 9319–9325.
39 S. Baroni, P. Giannozzi and E. Isaev, Density-functional perturbation theory for quasi-harmonic calculations, *Rev. Mineral. Geochem.*, 2010, **71**(1), 39–57.
40 J. S. Shah and M. E. Straumanis, Thermal expansion behavior of silicon at low temperatures, *Solid State Commun.*, 1972, **10**(1), 159–162.
41 S. Biernacki and M. Scheffler, Negative thermal expansion of diamond and zinc blende semiconductors, *Phys. Rev. Lett.*, 1989, **63**(3), 290–293.
42 Y. Zhang, Z. Wang, J. Xi and J. Yang, Temperature-dependent band gaps in several semiconductors: from the role of electron-phonon renormalization, *J. Phys.: Condens. Matter*, 2020, **32**(47), 475503.
43 F. Giustino, M. L. Cohen and S. G. Louie, Electron-phonon interaction using Wannier functions, *Phys. Rev. B*, 2007, **76**(16), 165108.
44 M. Zacharias, C. E. Patrick and F. Giustino, Stochastic approach to phonon-assisted optical absorption, *Phys. Rev. Lett.*, 2015, **115**(17), 177401.
45 H. Shang and J. Yang, The electron–phonon renormalization in the electronic structure calculation: Fundamentals, current status, and challenges, *J. Chem. Phys.*, 2023, **158**(13), 130901.
46 Y. P. Varshni, Temperature dependence of the energy gap in semiconductors, *Physica*, 1967, **34**(1), 149–154.
47 J. Bhosale, A. K. Ramdas, A. Burger, A. Muñoz, A. H. Romero, M. Cardona, R. Lauck and R. K. Kremer, Temperature dependence of band gaps in semiconductors: Electron-phonon interaction, *Phys. Rev. B*, 2012, **86**(19), 195208.
48 F. Giustino, Electron-phonon interactions from first principles, *Rev. Mod. Phys.*, 2017, **89**(1), 015003.
49 J. P. Nery, P. B. Allen, G. Antonius, L. Reining, A. Miglio and X. Gonze, Quasiparticles and phonon satellites in spectral functions of semiconductors and insulators: Cumulants applied to the full first-principles theory and the Fröhlich polaron, *Phys. Rev. B*, 2018, **97**(11), 115145.
50 A. Miglio, V. Brousseau-Couture, E. Godbout, G. Antonius, Y.-H. Chan, S. G. Louie, M. Côté, M. Giantomassi and X. Gonze, Predominance of non-adiabatic effects in zero-point renormalization of the electronic band gap, *npj Comput. Mater.*, 2020, **6**(1), 167.
51 S. Poncé, Y. Gillet, J. Laflamme Janssen, A. Marini, M. Verstraete and X. Gonze, Temperature dependence of the electronic structure of semiconductors and insulators, *J. Chem. Phys.*, 2015, **143**, 10.
52 M. Engel, H. Miranda, L. Chaput, A. Togo, C. Verdi, M. Marsman and G. Kresse, Zero-point renormalization of the band gap of semiconductors and insulators using the projector augmented wave method, *Phys. Rev. B*, 2022, **106**(9), 094316.
53 R. Pässler, Semi-empirical descriptions of temperature dependences of band gaps in semiconductors, *Phys. Status Solidi B*, 2003, **236**(3), 710–728.
54 M. Capdevila-Cortada, Z. Łodziana and N. López, Performance of DFT+U approaches in the study of catalytic materials, *ACS Catal.*, 2016, **6**(12), 8370–8379.
55 A. J. Bell, T. P. Comyn and T. J. Stevenson, Expanding the application space for piezoelectric materials, *APL Mater.*, 2021, **9**, 1.
56 P. Labéguerie, M. Harb, I. Baraille and M. Rérat, Structural, electronic, elastic, and piezoelectric properties of α-quartz and MXO_4 (M = Al, Ga, Fe; X = P, As) isomorph compounds: A DFT study, *Phys. Rev. B*, 2010, **81**(4), 045107.
57 L. Bellaiche and D. Vanderbilt, Virtual crystal approximation revisited: Application to dielectric and piezoelectric properties of perovskites, *Phys. Rev. B*, 2000, **61**(12), 7877–7882.